Effects of Reacting Flow on Continuum Breakdown in Hypersonic Aerothermodynamics

Timothy D. Holman[*] and Iain D. Boyd [†]

Department of Aerospace Engineering, University of Michigan, Ann Arbor, MI, 48109

This study investigates the effects of continuum breakdown on the surface aerothermodynamic properties (pressure, stress, heat transfer rate) of a sphere in Mach 25 flows in regimes varying from continuum to a rarefied gas. Results are generated using both continuum (CFD) and particle (DSMC) approaches. The DSMC method utilizes a chemistry model that calculates the backwards rates from an equilibrium constant. Tests of this model are run to confirm its validity and to compare it to the CFD chemistry model. The inclusion of reacting nitrogen flow did not significantly change the amount of continuum breakdown in the flow. Hence, there is little change in the maximum heat flux or the integrated drag on the surface of the sphere. The second part of this study examines the effect of reacting air flow on continuum breakdown and the surface properties of the sphere. As the global Knudsen number increases, the amount of continuum breakdown in the flow and on the surface increases. This increase in continuum breakdown significantly affects the surface properties, causing an increase in the differences between CFD and DSMC.

Nomenclature

a	Modified Arrhenius Rate Constant
$\bar{c}$	Mean Speed [m/s]
C_p	Pressure Coefficient
C_τ	Shear Coefficient
C_q	Heat Flux Coefficient
d	Molecular Diameter [m]
$f(g)$	Velocity Distribution Function
g	Relative Velocity [m/s]
k	Reaction Rate
K_e	Equilibrium Constant
Kn_∞	Global Knudsen Number
Kn_{GLL}	Gradient Length Local Knudsen Number
L	Characteristic Length [m]
U	Free Stream Velocity [m/s]
q	Heat Transfer Rate [W/m^2]
p	Pressure [Pa]
P	Average Probability
T	Translational Temperature [K]
Z	Collision Number
ε	Activation Energy [J]
λ	Mean Free Path [m]
μ	Viscosity [Pa·s]
ν	Mean Collision Rate [1/s]
η	Modified Arrhenius Temperature Power
γ	Ratio of Specific Heats

---

[*]Graduate Student, Member AIAA.
[†]Professor, Associate Fellow AIAA.

American Institute of Aeronautics and Astronautics

ρ	Density [kg/m^3]
ϕ	Instantaneous Probability
σ	Collision Cross Section [m^2]
τ	Shear Stress [Pa], Relaxation Time [s]
ω	VHS Temperature Exponent
ζ	Internal Degrees of Freedom

subscripts

BOLTZ	Boltzmann [1.38×10^{-23} J/K]
b	Backward
cont	Continuum
f	Forward
LT	Landau-Teller
p	Park
part	Particle
r	Rotation
REF	Reference Value
v	Vibration
VFD	Vibrationally Favored Dissociation
∞	Free Stream

I. Introduction

A hypersonic vehicle crosses many regimes from rarefied to continuum due to the change in density with altitude during the course of its trajectory through a planet's atmosphere. This variation makes it difficult to simulate the flow since the physical accuracy of computational fluid dynamics (CFD) can breakdown in rarefied flows and the direct simulation Monte Carlo (DSMC) method is computationally expensive in continuum flows. It is difficult and expensive to reproduce these varied flow conditions in ground based experiments and flight tests, so there is need for computational models that can be utilized for design and development of hypersonic vehicles.

The flow can be characterized by the Knudsen number as given in Eq. (1).

$$Kn = \frac{\lambda}{L} \propto \frac{1}{\rho L} \tag{1}$$

When the Knudsen number is much less than one the flow can be considered to be continuum and therefore should be simulated using traditional computational fluid dynamics techniques by numerically solving the Navier-Stokes equations. However, when the Knudsen number becomes larger, the continuum assumption in the Navier-Stokes equations starts to breakdown. This is due to the fact that these equations are derived from kinetic theory based on the assumption of small perturbations from an equilibrium velocity distribution function;[1] therefore CFD only works in near equilibrium flows. At higher altitudes, where the density is lower giving a larger Knudsen number, only a non-continuum technique can be used, such as the direct simulation Monte Carlo (DSMC) method.[2] In continuum flows over a blunt body, there can be locally rarefied flow in the shock, the boundary layer and the wake of the body. As a result, neither CFD nor DSMC can provide a complete computational model across all regimes of a hypersonic vehicle.

Since the flow around a body can locally be in breakdown, it is important to be able to identify areas of continuum breakdown. In order to identify the areas where the CFD method is in breakdown, the use of a continuum breakdown parameter is needed. Boyd, et al.[3] suggested the use of the maximum gradient length local Knudsen number as a continuum breakdown parameter given in Eq. (2).

$$Kn_{GLL} = \frac{\lambda}{Q} \left| \frac{dQ}{dl} \right| \tag{2}$$

where the derivative is taken in the direction of maximum gradient, and Q is a variable of interest such as density, temperature or pressure. It has been found that a value of Kn_{GLL} above 0.05 indicates continuum breakdown has occurred.

American Institute of Aeronautics and Astronautics

The DSMC method can be utilized in any dilute gas flow but becomes prohibitively expensive for low Knudsen number flows. In general, a CFD method is an order of magnitude faster than the DSMC method. Therefore, ways to extend the validity of CFD to higher Knudsen numbers is desirable. It has been found that replacing the no-slip boundary condition typically used in CFD with a velocity slip and temperature jump boundary condition can improve CFD in the transition regime.[4] However, if the flow is too far from continuum, the slip boundary conditions will not help the CFD method and a DSMC method is required for accurate simulation of the flow.

To be able to design a hypersonic vehicle it is important to be able to predict the surface properties on the vehicle. In order to do this, one must understand how continuum breakdown affects the surface conditions such as heat flux, pressure and shear stress. These surface conditions determine the aerodynamic and thermodynamic performance of a re-entry vehicle. A previous study by Lofthouse et al. looked at the effect of breakdown on the surface properties of a 12 inch diameter cylinder in a Mach 10 flow of argon.[5] Another study by Lofthouse et al. examines the effects of velocity slip and temperature jump at the surface of a 12 inch diameter cylinder in Mach 10 and 25 flow of argon.[4] Further work by Lofthouse et al. examines Mach 10 and 25 nitrogen flow over a cylinder.[6] This was extended to flow of nitrogen over a 12 inch sphere for Mach 10, 25 and 45 flow to be able to include a geometry that is more representative of re-entry vehicles.[7] To be able to accurately characterize continuum breakdown there is a need to start out with simple simulations and then add complexity to determine individual effects. The work done by Lofthouse et al. started this effort by characterizing breakdown over a two dimensional cylinder in a flow of argon and nitrogen. The present study will continue to examine the effects of continuum breakdown in Mach 25 flows of reacting nitrogen and air over a 12 inch diameter sphere in flow regimes from continuum to rarefied gas.

This paper will discuss the simulation procedures as well as the computational models used to perform the simulations. The paper will then discuss the surface properties as predicted by CFD and DSMC for the global Knudsen number of 0.01 case in reacting nitrogen flow and compare the results to the same case without reacting flow. A discussion of the surface properties predicted by CFD and DSMC in reacting air in several different flow regimes will follow. Finally, conclusions and future work are discussed.

II.   Numerical Methods

The DSMC simulations are performed using MONACO,[8] a code developed at University of Michigan by Boyd et al. MONACO is a parallel, unstructured, 2D/3D DSMC code, and it includes variable vibrational and rotational energy exchange models. The variable hard sphere (VHS) model[2] is employed in this study. The final mesh used for each simulation is adapted by hand from previous simulations such that the cell size is of the same order as the local mean free path.

For this study, a hybrid mesh, one with both structured and unstructured cells, with cell stretching is utilized. In this case, a structured grid with cell stretching is employed along the fore body surface while an unstructured mesh is used everywhere else in the flow field. This means the cell widths are adapted to be on the order of a mean free path while the cell heights are stretched larger than the mean free path. This procedure creates a larger cell volume so more particles can populate the cells near the stagnation point. This is important in axisymmetric simulations where it is difficult to obtain an appropriate number of particles per cell.[9] This does not affect the simulation results because the primary flow gradients along the stagnation line are aligned with the cell widths, which are small enough to properly simulate the flow.

The CFD simulations are performed by solving the Navier-Stokes equations by use of the Michigan aerothermodynamic Navier-Stokes code LeMANS, developed at the University of Michigan for the simulation of hypersonic reacting flows.[10,11] LeMANS is a parallel, unstructured 2D/3D, finite-volume CFD code. LeMANS has the ability to simulate gases in chemical, rotational and vibrational nonequilibrium. LeMANS employs a modified Steger-Warming Flux Vector Splitting to discretize the numerical fluxes between cells, which has low dissipation and is appropriate near boundary layers. A line implicit method is employed for the time integration. Even though LeMANS can handle unstructured meshes, all the simulations performed for this study are carried out using structured meshes. It is necessary to ensure that the transport properties are the same in both CFD and DSMC; therefore LeMANS is modified to use the same viscosity as the VHS method as given in Eqs. (3) and (4).[12]

$$\mu = \mu_{ref} \left(\frac{T}{T_{ref}} \right)^{\omega} \tag{3}$$

American Institute of Aeronautics and Astronautics

$$\mu_{ref} = \frac{15\sqrt{\pi m k_{BOLTZ} T_{ref}}}{2\pi d_{ref}^2 (5 - 2\omega)(7 - 2\omega)} \tag{4}$$

where the variable hard sphere parameters are the same as those used in the DSMC simulations. However, in the CFD method the viscosity that is used is the average of the species viscosities.

II.A.   Vibrational Relaxation

There are two models for the exchange of vibrational and translational energy in DSMC, the first is a phenomenological model as described by Boyd.[13] The probability of an inelastic collision where vibrational energy is exchanged with translational energy is proportional to the inverse of the vibrational relaxation time. This probability is the average over the instantaneous probabilities as shown in Eq. (5)

$$P = \frac{1}{\tau_v \nu} = \int_0^\infty \phi(g) f(g) \, dg \tag{5}$$

where $\phi(g)$ is the instantaneous probability for a given relative velocity and velocity distribution function.

To approximate the vibrational relaxation time, a Landau-Teller model is utilized with correlated experimental data from Millikan and White,[14] as expressed in Eq. (6)

$$\tau_{LT} = \frac{1}{p} exp\left[A\left(T^{-\frac{1}{3}} - B\right) - 18.42\right] \tag{6}$$

where the pressure is in atm. For this study, the values of A and B come from Park[15] for both DSMC and CFD. To be able to utilize the above model, a modified Landau-Teller form is found, as shown in Eq. (7)

$$\phi_{LT} = \frac{1}{Z_0} g^\alpha \exp\left(\frac{-g^*}{g}\right) \tag{7}$$

where the constants are found to satisfy Eq. (5). Unfortunately this integral cannot be evaluated analytically so the method of steepest descent is employed. For high temperatures, which are often encountered in hypersonic flows, a correction proposed by Park[16] is used as shown in Eq. (8)

$$\tau_P = \frac{1}{n\bar{c}\sigma} \tag{8}$$

where σ is the collision cross section, $\bar{c}$ is the mean thermal speed and n is the number density. An instantaneous probability for Park's correction can be derived in a similar manner as done for the Landau-Teller model. The total vibrational relaxation time is the sum of the Landau-Teller and Park relaxation times. The total instantaneous probability is given by Eq (9)

$$\phi(g) = \frac{\phi_{LT}\phi_P}{\phi_{LT} + \phi_P} \tag{9}$$

A factor was proposed by Lumpkin et al. to correct the DSMC relaxation time.[17] Although this was done for rotational relaxation, it can also be applied to vibration relaxation, as shown in Eq. (10)

$$\tau_{part} = \frac{\tau_{cont}}{1 + \frac{\zeta}{4 - 2\omega}} \tag{10}$$

When the instantaneous probability is integrated over all collisions, it should match the average probability calculated from theory; however, it was found in a previous study[18] that they do not match. It is thought that the probabilities do not match due to the method of steepest descent required to find the instantaneous probability. It has been found that the probability can better correspond with theory by multiplying by a simple factor that is dependent on the maximum temperature.[6]

Unfortunately, this method does not work for multiple species, and in fact was only employed for N_2-N_2 vibrational relaxation.[6,7] For multiple species, a more elegant solution has been included in the DSMC method to be able to obtain the proper vibrational relaxation rate. The problem of having to calculate the instantaneous probability for every collision can be avoided by simply calculating the vibrational relaxation time for each collision class for each cell as discussed by Deschenes et al.[19] The probability for each collision

class and each cell can then be calculated using Eq. (5). The vibrational relaxation time can be calculated by using Landau-Teller model, Eq.(6), and Park, Eq. (8). A factor proposed by Gimelshein et al.[20] is needed to be able to utilize this relaxation time in a particle simulation as shown in Eq. (11)

$$\tau_{part} = \frac{\tau_{cont}}{1 + \frac{0.5\,\zeta^2 exp\left(\frac{\theta_v}{T}\right)}{4 - 2\omega}} \qquad (11)$$

This model in DSMC was shown by Deschenes et al. to match the vibrational relaxation in CFD for nitrogen.[19] Since this model has only been tested with one species, a heat bath of 5 species air is run with the cell based model and the phenomenological model in DSMC and compared to CFD. The heat bath is started with a translational temperature of 15,000 K while rotational and vibrational temperatures are started at 10,000 K. From the results of this test, which are displayed in Fig. 1, it can be seen that the cell based method is in better agreement with CFD than the variable vibration probability.
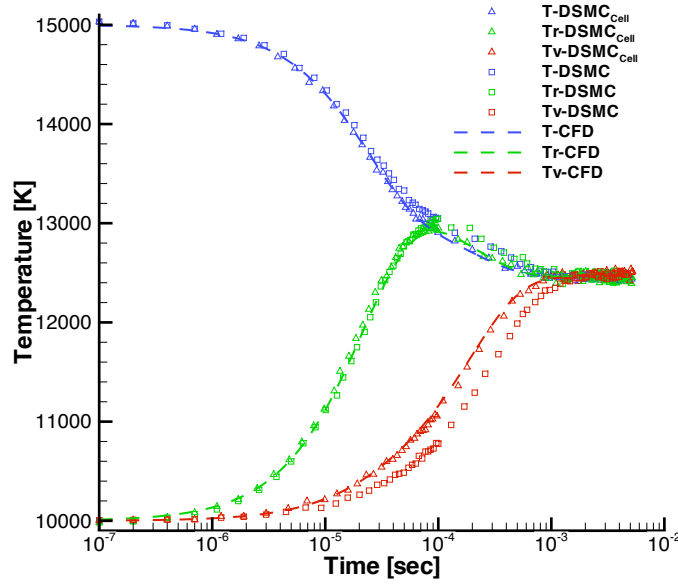

Figure 1. Comparison of Thermal Relaxation Process as Predicted by DSMC and CFD in 5 Species Air

II.B. Chemical Equilibrium

In the DSMC method, a collision pair is selected and the probability of reaction is compared to a random number. If the probability is greater than the random number then a reaction occurs. Once a reaction occurs, a Borgnakke-Larsen model is applied to be able to distribute the energy to the available energy modes. There are two models available in MONACO for chemistry; the total collision energy (TCE) model and the vibrationally favored dissociation (VFD) model.[21] The VFD model is employed in the DSMC method for this study, and a qualitatively similar model is used in the CFD method. For both the TCE and VFD models, the reaction rate, forward or backward, must be in modified Arrhenius form. The probability of reaction is found by integration of the equilibrium Boltzmann distribution function as shown in Eq. (12).

$$k_f(T) = a_f T^{\eta_f} \exp\left(\frac{-\varepsilon_f}{k_{BOLTZ}T}\right) = \langle\sigma g\rangle \int_{\varepsilon_f}^{\infty} P_c(\varepsilon_c) \int_{\varepsilon_v=0}^{\infty} P_v(\varepsilon_v) f_B(\varepsilon_v) f_B(\varepsilon_c - \varepsilon_v)\, d\varepsilon_v\, d\varepsilon_c \qquad (12)$$

where f_B is the equilibrium Boltzmann distribution for energy. Since the reaction rate has the modified Arrhenius form, the reaction probability for the VFD model is found to be

$$P_{VFD} = A \left(\frac{\varepsilon_v}{\varepsilon_c}\right)^{\phi} \frac{(\varepsilon_c - \varepsilon_f)^{\psi}}{(\varepsilon_c)^{\chi}} \qquad (13)$$

American Institute of Aeronautics and Astronautics

where A is a complicated constant not reproduced here, ϕ is a constant dependent upon the species,[22] $\psi = \eta + 0.5 + \zeta$ and $\chi = 1 + \zeta - \omega$. If ϕ is set to zero the total collision energy model is recovered from the VFD model.

In order to have backward reactions in the VFD model, the rate coefficient must be in the modified Arrhenius form. The backward rates are calculated using the forward rates and the equilibrium constant, as shown in Eq. (14)

$$k_b(T) = \frac{k_f(T)}{K_e(T)} = a_b T^{\eta_b} \exp\left(\frac{-\varepsilon_b}{k_{BOLTZ}T}\right) \tag{14}$$

Typically in the DSMC method, the backward rates are fit to a modified Arrhenius form over a specified temperature range.[23] This can cause problems if a simulation goes outside this temperature range and all the fits need to be redone. With the growth of hybrid methods, it is necessary for the DSMC method to match the CFD method, and it is also important for this study. It is common in the CFD method to use a line fit proposed by Park[16] to find the equilibrium constant, as given in Eq. (15). This equilibrium constant is then applied to find the backward reaction rate.

$$K_e(T) = \exp\left[A_1\left(\frac{T}{10000}\right) + A_2 + A_3\ln\left(\frac{10000}{T}\right) + A_4\left(\frac{10000}{T}\right) + A_5\left(\frac{10000}{T}\right)^2\right] \tag{15}$$

The constants, A_i, are dependent on the number density as given by Park.[16] The constants are found using an interpolation method if the number density is within the range of the data. If the number density falls outside of that range the constants at the highest or lowest points are used accordingly. Instead of performing a fit over a limited temperature range, it would be desirable to evaluate the equilibrium constant, and then calculate the backwards reaction rates. This can be done by a method suggested by Boyd,[21] that utilizes the equilibrium constant and maintains the modified Arrhenius form required by the DSMC chemistry model. The backward reaction rate is found by taking the forward reaction rate, Eq. (12), and substituting into Eq. (14), since $\eta_b = \eta_f$ one can solve for the backward rate constant as shown in Eq. (16).

$$a_b = \frac{a_f}{K_e(T)}\exp\left(\frac{-\varepsilon_f}{k_{BOLTZ}T}\right) \tag{16}$$

This can now be substituted into the modified Arrhenius form and the probability for the backwards reaction can be found in the same way as described for the forward reaction. To test this model, a heat bath simulation is performed. The first test case is with nitrogen and the second is with air, both starting at a temperature of 15000 K. The results of these test cases are given in Fig. 2. The figure gives the density profiles over time for DSMC, the original model and the new equilibrium model, and CFD. From the first figure it can be seen that both DSMC models compare very well with each other and CFD for a simple two species nitrogen model. When a five species air model is tested it can be seen there are some transient differences in the middle, but all species approach similar values as the system nears equilibrium. The temperature profiles from the air heat bath test case are given in Fig. 2 (c). From this figure it is seen that the two methods predict different temperature profiles. In some instances the temperatures are different by approximately 2000 K but converge to similar values as the system approaches equilibrium. The difference in the species densities might be caused by the differences seen in the temperature profile, since the chemical rates are temperature dependent.

With Park's equilibrium model now being utilized in the DSMC method, the equilibrium constant in both CFD and DSMC are calculated in the same manner. Since the equilibrium constants are the same for DSMC and CFD, the backward reaction rates are also the same for both methods if the temperature is the same. However, there are still many fundamental differences in the chemistry models employed in CFD and DSMC. For instance, both methods utilize a model for favorably dissociating molecules with higher vibrational energies. Unfortunately, the models employed by the two methods are different and are only quantitatively similar. This also ties into how the energy is distributed among the components of energy when reactions are occurring. DSMC employs a Larsen-Borgnakke method to distribute energy, while CFD relies on the species source terms and the energy conservation equations to distribute energy. The preferential dissociation of particles with higher vibrational energy in CFD is handled by modifying the source term in the vibrational energy conservation equation. These differences between the two methods need to be studied in more detail to fully understand the impact reacting flow has on continuum breakdown.
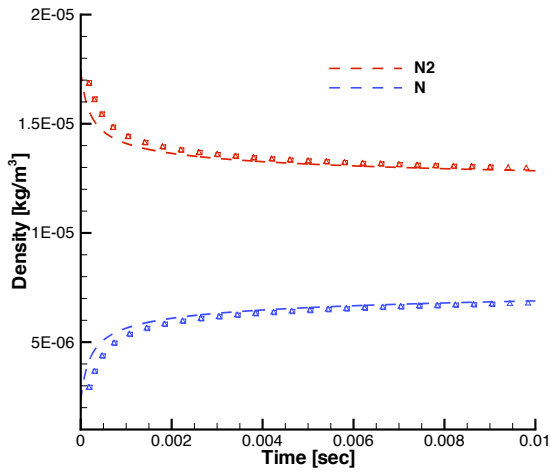
(a) Nitrogen
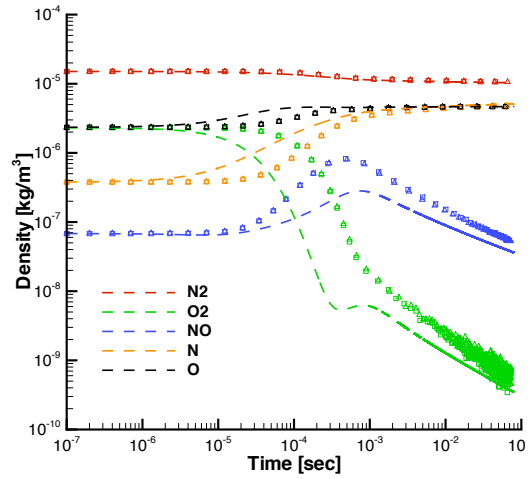
(b) Air
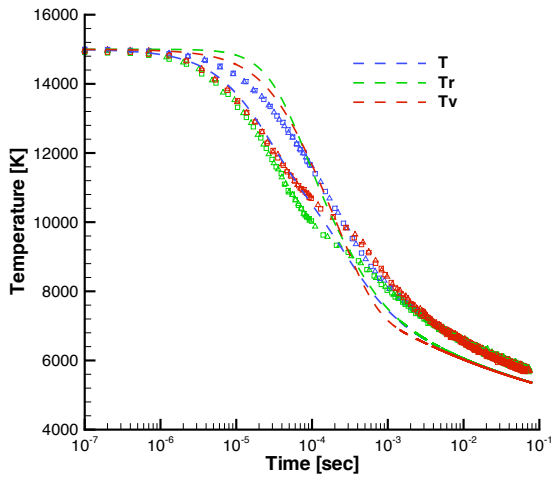
(c) Air Temperature

Figure 2. Comparison of Chemical Reaction Process as Predicted by DSMC and CFD in Nitrogen and Air; Triangles Represent DSMC with Park's Equilibrium, Squares Represent DSMC and Lines Represent CFD

American Institute of Aeronautics and Astronautics

III.   Flow Conditions

This study examines continuum breakdown in Mach 25 flows of reacting nitrogen and air over a 12 inch diameter sphere. The free stream temperature is 200 K giving free stream velocities of 7209 m/s and 7108 m/s for nitrogen and air, respectively. The surface of the sphere has a fixed temperature of 1500 K. The density of the free stream is varied to change the global Knudsen number of the flow from continuum to a rarefied gas as given in Table 1. The Knudsen number is calculated using the diameter of the sphere as the characteristic length and the hard sphere model to calculate the mean free path. The gray row gives the conditions for nitrogen, while the rest of the table gives the conditions for air.

Table 1. Simulated flow regimes

Kn_∞	Mass Density (kg/m^3)	Number Density ($particles/m^3$)	Mean Free Path (m)
0.01	1.975×10^{-5}	4.247×10^{20}	3.048×10^{-3}
0.002	1.007×10^{-4}	2.103×10^{21}	6.096×10^{-4}
0.01	2.014×10^{-5}	4.206×10^{20}	3.048×10^{-3}
0.05	3.987×10^{-6}	8.325×10^{19}	1.524×10^{-2}
0.25	8.057×10^{-7}	1.680×10^{19}	7.620×10^{-2}

IV.   Results

The purpose of this study is to compare surface properties predicted by DSMC and CFD simulations, heat flux, pressure and shear stress, to see if any differences occur due to continuum breakdown. Additionally, the integrated drag and the maximum heat flux are also compared from DSMC and CFD. The maximum heat flux is found by averaging the heat flux over the surface of the sphere within the first degree of the stagnation point. This is done to be able to determine the maximum heat flux predicted by DSMC which can have some random noise in the results. Since the CFD solutions are smooth, there is no need for averaging and the maximum heat flux is found by finding the maximum value of the heat flux on the surface of the sphere.

The breakdown parameter is computed from both DSMC and CFD simulation results using Eq.(2), where the derivative is taken in the direction of the maximum gradient. It is expected that continuum breakdown will occur in areas of high gradients, in the shock wave and boundary layer, and in areas of rarefied gas flow in the wake.

The results that are presented in this paper for the surface aerothermodynamic properties are given as non-dimensionalized coefficients which are defined by Eqs. (17 - 19).

$$C_p = \frac{p - p_\infty}{\frac{1}{2}\rho_\infty U_\infty^2} \tag{17}$$

$$C_\tau = \frac{\tau}{\frac{1}{2}\rho_\infty U_\infty^2} \tag{18}$$

$$C_q = \frac{q}{\frac{1}{2}\rho_\infty U_\infty^3} \tag{19}$$

The surface aerothermodynamic properties are plotted against the surface angle ϕ, which is measured from the stagnation point.

IV.A.   Reacting Nitrogen Flow

First, the results for a Mach 25 reacting nitrogen flow at global Knudsen number of 0.01 are discussed and compared to a case without chemical reactions from a previous study.[7] The reason for this is to be able to discern the effects of including reacting flow on continuum breakdown and the surface properties. This case involves two reactions for the dissociation of nitrogen: the reaction rates are the first two given in Table 6. This is a simple way to start the comparisons of reacting flow. In the next section more complexity is incorporated with additional species and reactions. The integrated drag and the peak heat flux values

American Institute of Aeronautics and Astronautics

predicted by DSMC and CFD, with and without slip boundary conditions, are given in Tables 2 and 3. From Table 2 it is seen that the inclusion of reacting flow has almost no effect on the integrated drag. However, it can be seen, in Table 3, that including reacting flow lowers the peak heating but has little effect on the comparison between CFD and DSMC. The behavior of the peak heating is an expected trend: it takes energy for a reaction to occur lowering the energy in the flow and causing a decrease in the peak heating. Eventually all the dissociated atoms will recombine to molecules releasing that energy back into the flow, but this happens after the flow has moved away from the stagnation point.

Table 2. Integrated Drag [N] (%$difference$) from DSMC and CFD for Mach 25 Flow

	Kn_∞	DSMC	CFD (no-slip)	CFD (Gökçen)
Chemistry	0.01	41.12	42.39(3.09%)	41.25(0.33%)
No Chemistry	0.01	41.2	42.44(2.99%)	40.34(-2.09%)

Table 3. Peak Heating $\left[\frac{W}{m^2}\right]$ (%$difference$) from DSMC and CFD for Mach 25 Flow

	Kn_∞	DSMC	CFD (no-slip)	CFD (Gökçen)
Chemistry	0.01	9.63×10^5	$1.04\times10^6(7.92\%)$	$9.96\times10^5(3.37\%)$
No Chemistry	0.01	9.81×10^5	$1.08\times10^6(10.22\%)$	$1.03\times10^6(4.87\%)$

The gradient length local Knudsen number contours for DSMC and CFD are given in Fig. 3 (a). This figure gives the contours of Kn_{GLL} for the simulation with reacting flow, shown as flood, along with the contours without reacting flow, given as lines. It can be observed that there is almost no difference in the amount of continuum breakdown between the simulations with and without reacting flow in both CFD and DSMC. The data seen in Tables 2 and 3 can be explained by the fact that the amount of breakdown has not significantly changed with the inclusion of chemistry. The reason there has been relatively little change with the addition of chemistry is due to the small amount of dissociation that is occurring at this condition. The maximum mass fraction of atomic nitrogen is just 0.03, making this simulation mostly molecular nitrogen.
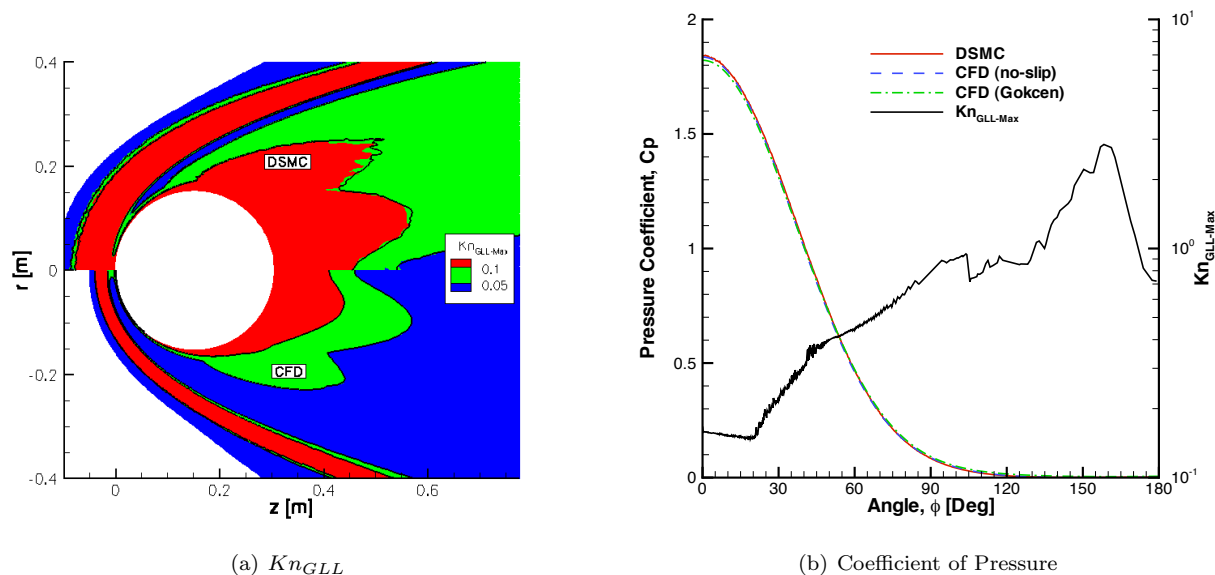

(a) Kn_{GLL}

(b) Coefficient of Pressure

Figure 3. $Kn_\infty = 0.01$, Kn_{GLL} contours, surface pressure (left axis) and Kn_{GLL} surface profile (right axis) on a sphere in a Mach 25 flow of reacting nitrogen

The pressure coefficient over the surface of the sphere is given in Fig. 3 (b), along with the surface profile of Kn_{GLL}. From the figure it can be seen that the gradient length local Knudsen number is above the threshold value of 0.05, indicating that the flow on the surface is in breakdown. Even though the flow along the surface is in breakdown, the surface pressure predicted by the two methods agree very well: all three
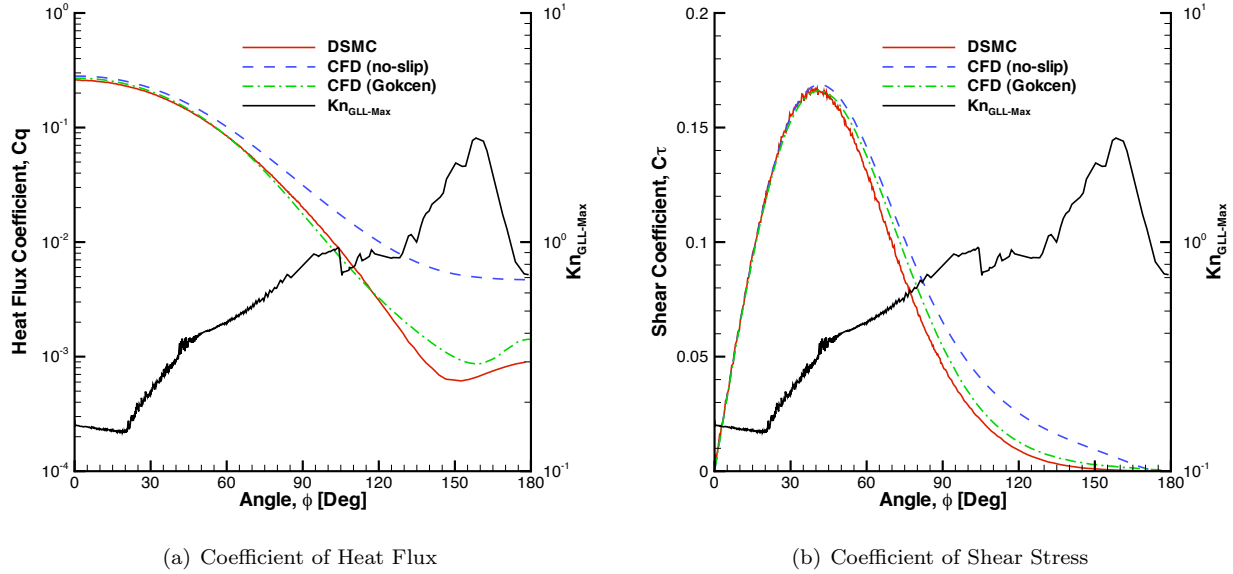
American Institute of Aeronautics and Astronautics

(a) Coefficient of Heat Flux   (b) Coefficient of Shear Stress

Figure 4. $Kn_\infty = 0.01$, **surface heat flux (left axis), surface shear stress (left axis) and** Kn_{GLL} **surface profile (right axis) on a sphere in a Mach 25 flow of reacting nitrogen**

curves lie nearly on top of each other. The surface heat flux coefficient is given in Fig. 4 (a). The CFD with no slip boundary conditions predicts a higher heat flux over the entire surface. This is not surprising given the entire surface is considered to be in breakdown. However, slip boundary conditions in CFD improve the heat flux prediction in comparison to DSMC. The shear stress coefficient given in Fig. 4 (b), displays good agreement between the two techniques. There is a slight divergence over the aft of the sphere from the results predicted with the CFD with no-slip boundary conditions, but slip boundary conditions in CFD improve the agreement with DSMC.

IV.B.   Reacting Air Flow

The next step in this study considers Mach 25 flow of 5 species reacting air over a sphere with a global Knudsen number varying from 0.002 to 0.25. This portion of the study aims to characterize the effects of continuum breakdown, in a flow more reminiscent of a real gas. This case involves 17 reactions, which includes dissociation and exchange reactions; the reaction rates are given in Table 6. The integrated drag, peak heat flux and percent difference between DSMC and CFD are given in Tables 4 and 5, respectively. Since DSMC is a particle method that works in both the continuum regime and the rarefied regime, it is assumed that the DSMC results are more accurate, so the percent difference is calculated using the DSMC result as the correct result.

Table 4.   Integrated Drag [N] ($\%difference$) **from DSMC and CFD for Mach 25 Flow in Reacting Air**

Kn_∞	DSMC	CFD (no-slip)	CFD (Gökçen)
0.002	176.71	175.68(-0.58%)	174.56(-1.22%)
0.01	40.85	41.99(2.78%)	40.67(-0.45%)
0.25	2.58	5.18(101.22%)	2.81(9.03%)

From these tables it can be seen that the comparisons between CFD and DSMC diverge with growing global Knudsen number. In the following subsections, the surface properties and gradient length local Knudsen number are discussed in more detail for each case.

IV.B.1. $Kn_\infty = 0.002$

Given the global Knudsen number, the flow is expected to be in the continuum regime. However, there are regions of local continuum breakdown in the shock and wake regions as shown in Fig. 5 (a). There is a larger

American Institute of Aeronautics and Astronautics

Table 5. Peak Heating $\left[\frac{W}{m^2}\right]$ (%difference) from DSMC and CFD for Mach 25 Flow in Reacting Air

Kn_∞	DSMC	CFD (no-slip)	CFD (Gökçen)
0.002	9.39×10^5	$9.88\times10^5(3.94\%)$	$9.70\times10^5(1.84\%)$
0.01	7.88×10^5	$9.35\times10^5(18.77\%)$	$8.78\times10^5(11.52\%)$
0.25	1.08×10^5	$1.85\times10^5(70.84\%)$	$9.22\times10^4(-14.86\%)$

area of continuum breakdown observed in DSMC over CFD in both the shock region and in the wake region behind the sphere.

(a) Kn_{GLL}

(b) Coefficient of Pressure
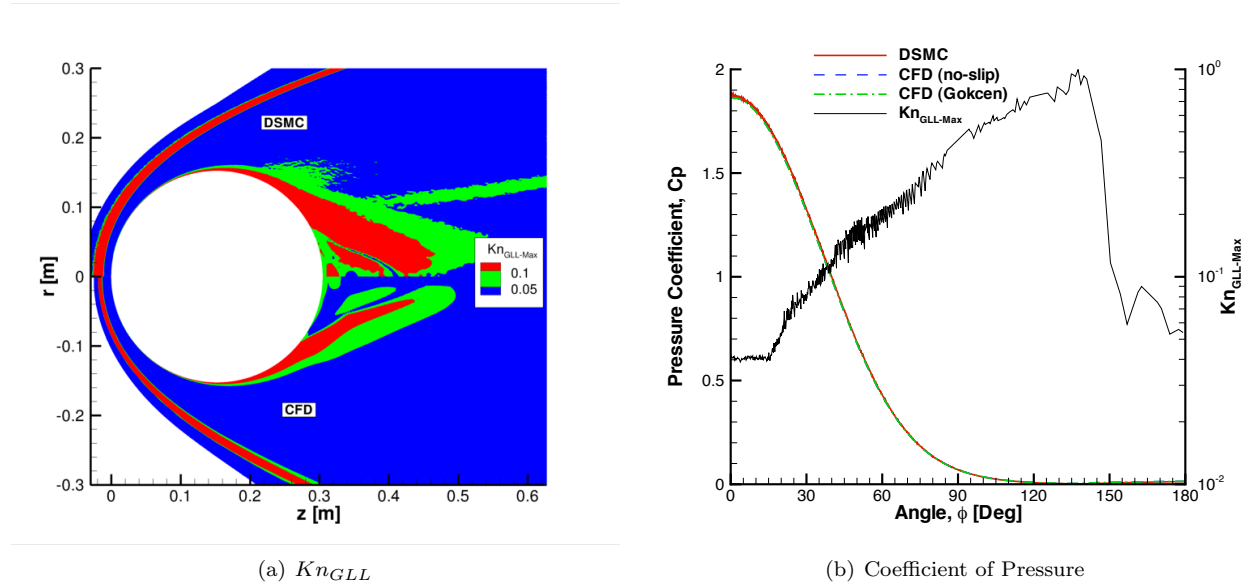
Figure 5. $Kn_\infty = 0.002$, Kn_{GLL} contours, surface pressure (left axis) and Kn_{GLL} surface profile (right axis) on a sphere in a Mach 25 flow of reacting air

The surface pressure coefficient is given in Fig. 5 (b), along with the surface profile of Kn_{GLL}. Notice that Kn_{GLL} is above 0.05 for nearly the entire surface. Even at a global Knudsen number of 0.002, the flow at the surface is considered to be in breakdown. Despite the breakdown at the surface, the pressures predicted by DSMC and CFD match very well, with the three curves being nearly indistinguishable from each other. The surface heat flux predicted by CFD compares well with DSMC over the fore body of the sphere, as shown in Fig 6 (a). The divergence in the solution may be caused by the breakdown on the surface, especially over the aft of the sphere. The shear stress over the surface of the sphere is given in Fig. 6 (b). The shear stress prediction given by CFD compares well with DSMC over the surface, with only slight disagreement in the aft of the sphere. Slip boundary conditions in CFD improves the agreement with DSMC in the aft of the sphere.

To determine the level of chemistry occurring in the flow, the mass fractions of each species are given in Fig. 7 (a). It should be noted that in DSMC, the diffusion of species out from behind the shock is well known. This phenomenon can be seen by the large discrepancies between CFD and DSMC in mass fraction for nitric oxide, atomic oxygen and atomic nitrogen that develop moving away from the stagnation point. From the figure it can be seen that the mass fractions predicted by the two methods compare well, the only noticeable difference is in the mass fraction for nitric oxide. It can be seen that the minimum mass fraction of N_2 is approximately 0.5 while the maximum of N is 0.28, meaning nearly all of the dissociated nitrogen stays as atomic nitrogen. The same observation can be made of oxygen, meaning very little nitric oxide is created or destroyed with the exchange reactions. The temperature and gradient length local Knudsen number profile along the stagnation streamline is given in Fig. 7 (b). It can be observed that the translational temperature matches well between the two codes. However, the rotational and vibrational temperatures do not match as well. The over prediction of rotational temperature by CFD as compared to DSMC is an expected result,
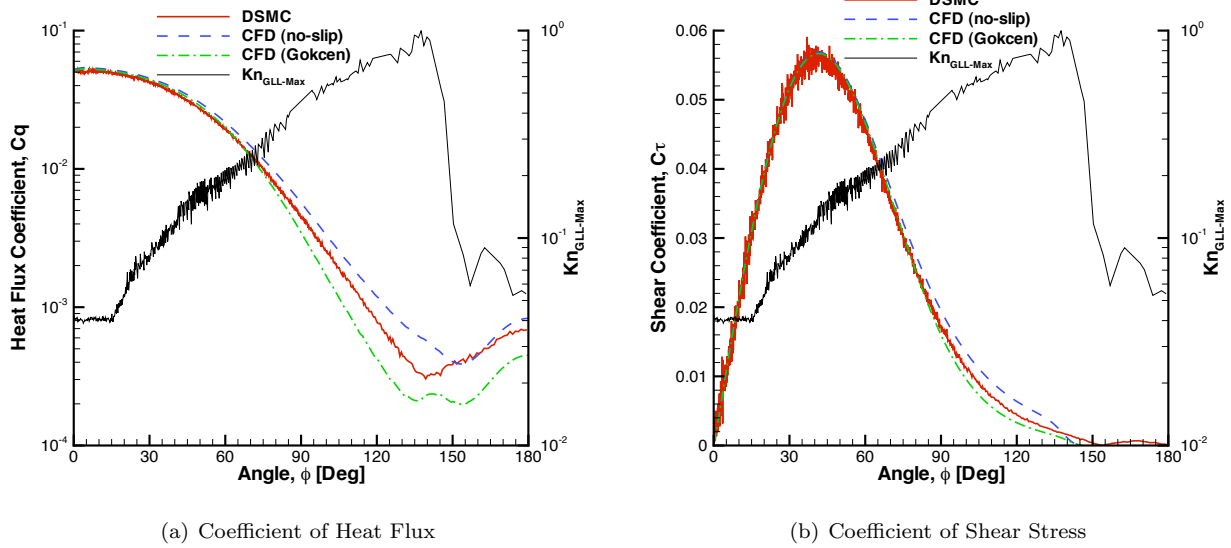
American Institute of Aeronautics and Astronautics

(a) Coefficient of Heat Flux

(b) Coefficient of Shear Stress

Figure 6. $Kn_\infty = 0.002$, surface heat flux (left axis), surface shear stress (left axis) and Kn_{GLL} surface profile (right axis) on a sphere in a Mach 25 flow of reacting air

however the over prediction of the vibrational temperature by DSMC as compared to CFD is not expected. From the profile of Kn_{GLL} it is seen that the flow is expected to be in the continuum regime as it approaches the wall. This means the difference in vibrational temperature is probably caused by differences in the way the energy distribution is handled in the two methods.

(a) Mass Fraction
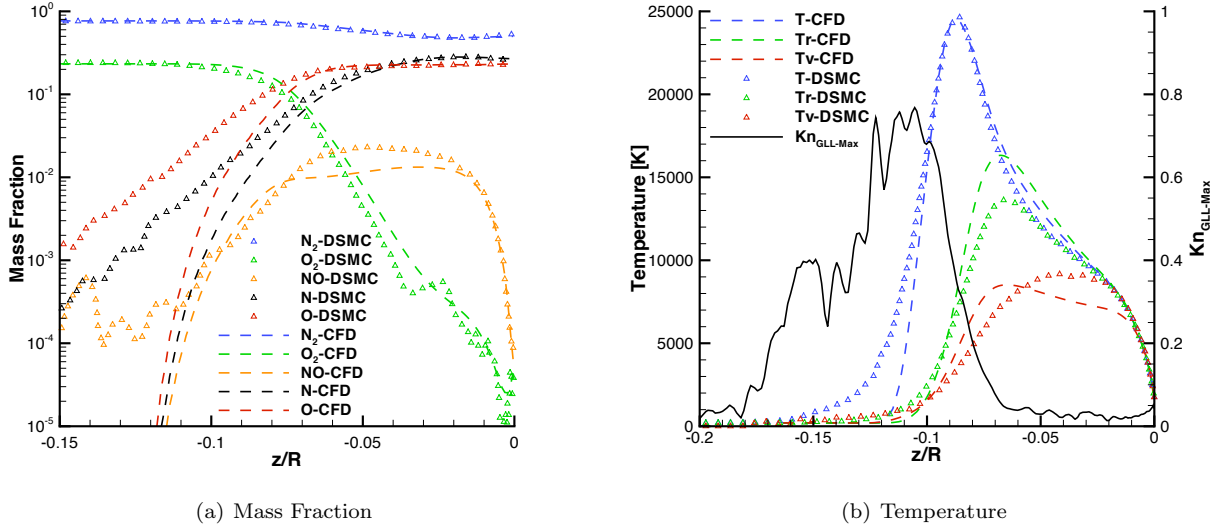
(b) Temperature

Figure 7. $Kn_\infty = 0.002$, temperature (left axis), mass fraction (left axis) and Kn_{GLL} (right axis) profiles along the stagnation streamline in a Mach 25 flow of reacting air

IV.B.2. $Kn_\infty = 0.01$

At a global Knudsen number of 0.01, the traditional limit for accurate CFD simulations, there is significant breakdown in the shock, boundary layer and the wake regions of the flow, as seen in Fig. 8 (a). At this condition the amount of breakdown is larger in DSMC than in CFD. Also, the shock is much thicker in DSMC than CFD, while the shock location is approximately the same. Notice that the flow is in breakdown all the way from the shock to the surface of the sphere near the stagnation streamline.

American Institute of Aeronautics and Astronautics
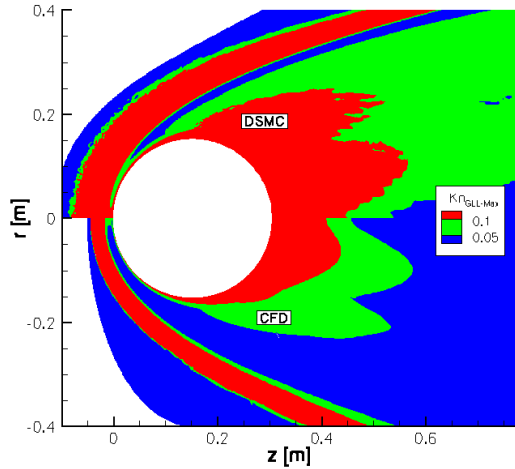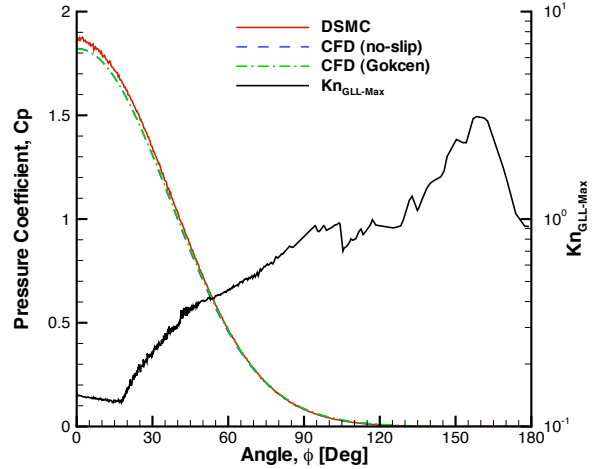
(a) Kn_{GLL}

(b) Coefficient of Pressure

Figure 8. $Kn_\infty = 0.01$, Kn_{GLL} **contours, surface pressure (left axis) and** Kn_{GLL} **surface profile (right axis) on a sphere in a Mach 25 flow of reacting air**

The surface pressures predicted from CFD and DSMC are still in good agreement despite the higher global Knudsen number, as shown in Fig. 8 (b). This figure also includes the surface profile of the gradient length local Knudsen number which shows the flow over the entire surface is in breakdown. The fact that the flow is in breakdown from the shock to the surface may have caused the slight discrepancy seen in the pressure coefficient near the stagnation point. The heat flux predicted by CFD with no-slip is always larger than DSMC over the entire surface, as can be seen in Fig. 9 (a). An improvement is seen if slip boundary conditions are employed in the CFD method, although this slightly under predicts the heat flux over the aft of the sphere. The surface shear stress coefficient compares well between DSMC and CFD without slip over the fore body of the sphere, as shown in Fig. 9 (b). Again, there is an improvement in the results when slip boundary conditions are used in the CFD method.
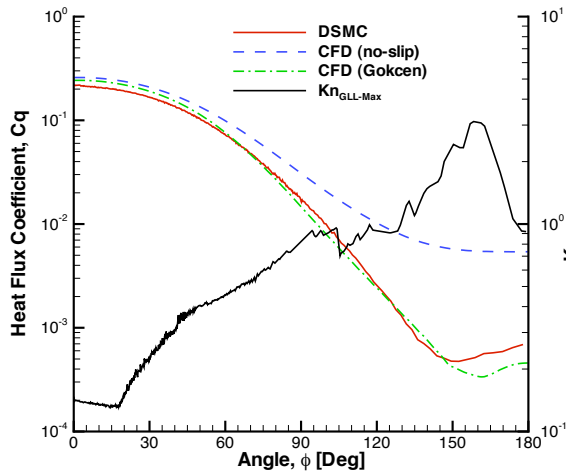
(a) Coefficient of Heat Flux
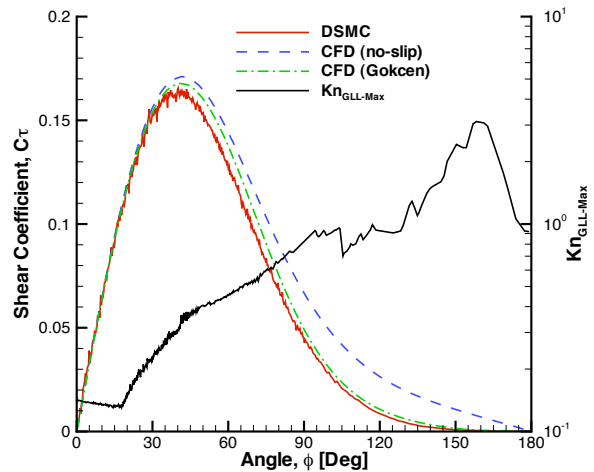
(b) Coefficient of Shear Stress

Figure 9. $Kn_\infty = 0.01$, **surface heat flux (left axis), surface shear stress (left axis) and** Kn_{GLL} **surface profile (right axis) on a sphere in a Mach 25 flow of reacting air**

To be able to determine the level of chemistry occurring in the flow, the mass fractions of each species

are given in Fig. 10 (a). Again, the large discrepancies between CFD and DSMC in mass fraction for nitric oxide, atomic oxygen and atomic nitrogen that develop moving away from the stagnation point are caused by diffusion in DSMC. From this figure it can be seen that molecular oxygen has dissociated while molecular nitrogen has undergone little change. There is a negligible amount of atomic nitrogen and nitric oxide that has been created behind the shock, with approximately 0.03 and 0.02 mass fractions, respectively. It is an expected result that molecular oxygen dissociated more easily due to a weaker bond as compared to molecular nitrogen. The profile for the temperatures and gradient length local Knudsen number along the stagnation streamline are given in Fig. 10 (b). Since DSMC has a thicker shock it can be seen that the temperature starts rising earlier then CFD. The flow is forced into thermal equilibrium as it moves closer to the wall, but CFD overshoots the DSMC temperatures prior to reaching equilibrium. This situation has been seen in a previous study,[7] and is caused by the fact that the flow is in nonequilibrium following the shock.
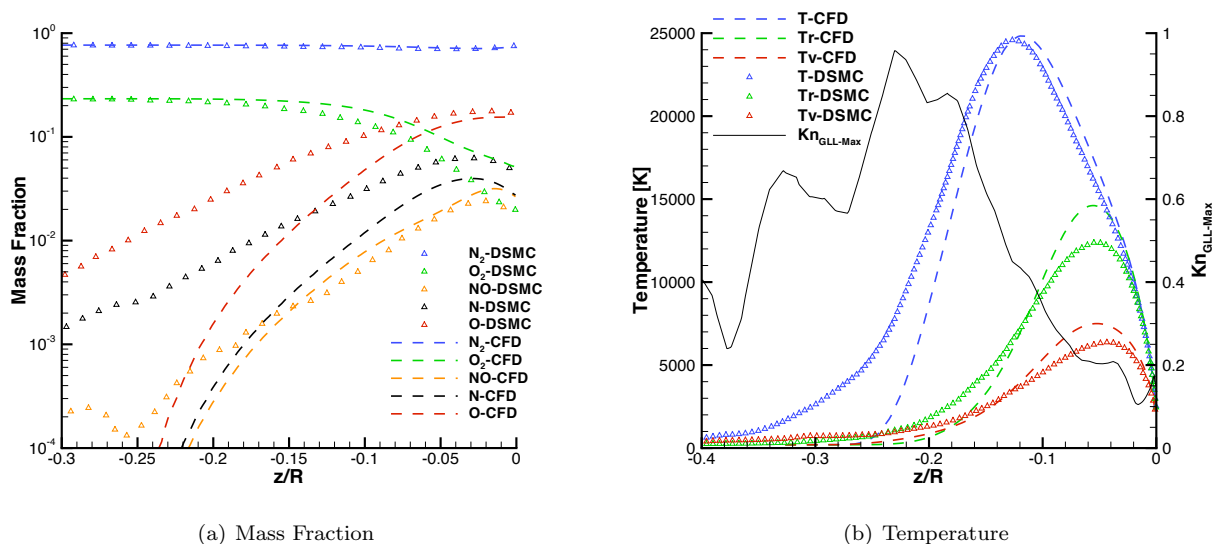

(a) Mass Fraction

(b) Temperature

Figure 10. $Kn_\infty = 0.01$, **temperature (left axis), mass fraction (left axis) and** Kn_{GLL} **(right axis) profiles along the stagnation streamline in a Mach 25 flow of reacting air**

*IV.B.3.* $Kn_\infty = 0.25$

The highest global Knudsen number considered in this study is 0.25. At this Knudsen number, the flow is in the rarefied regime, outside the range of where the CFD method should be employed. At this high of a global Knudsen number, the entire flow is in continuum breakdown, as seen in Fig. 11 (a). The shock standoff distance in DSMC is farther out than in CFD, almost twice the distance in DSMC as compared to CFD.

At this condition, continuum breakdown, has a strong effect on the surface properties. The surface pressure coefficient is given in Fig. 11 (b), along with the surface profile of gradient length local Knudsen number. As expected, the entire surface is considered to be in breakdown. The surface pressure coefficient is over predicted by CFD, with or without slip, as compared to DSMC. The surface heat flux coefficient shows very poor agreement between CFD and DSMC, as shown in Fig. 12 (a). When slip boundary conditions are employed in the CFD method there is an improvement in the results as compared to DSMC, but there is still approximately 4 orders of magnitude difference between CFD and DSMC in the aft of the sphere. The shear stress is under predicated by CFD with slip and over predicted by CFD without slip as compared to DSMC, as shown in Fig. 12 (b). Notice that the location of peak shear stress predicated by CFD with slip is approximately in the same location as DSMC, while the location predicted by CFD without slip occurs further back on the surface of the sphere.

The mass fraction for each species along the stagnation streamline for this flow condition are given in Fig. 13 (a). At this high of a global Knudsen number, there has been little change in the mass fractions for molecular oxygen and nitrogen. As a result there is negligible amounts of nitric oxide, atomic nitrogen
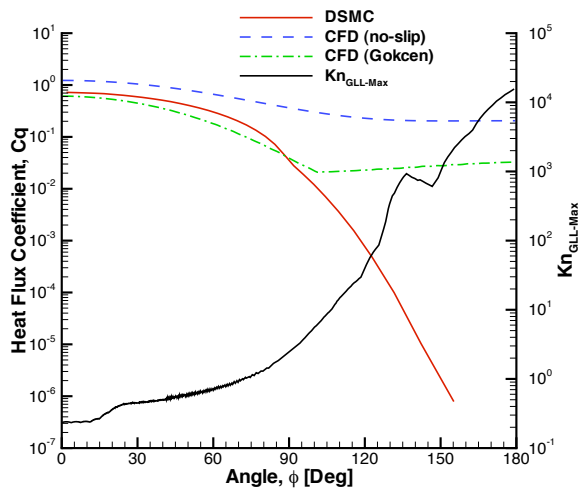
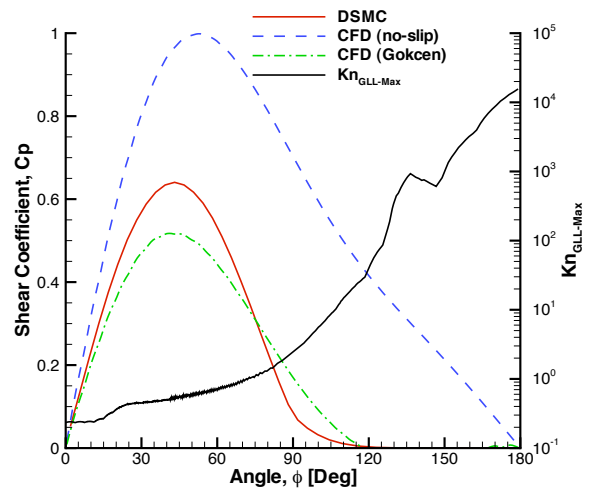American Institute of Aeronautics and Astronautics
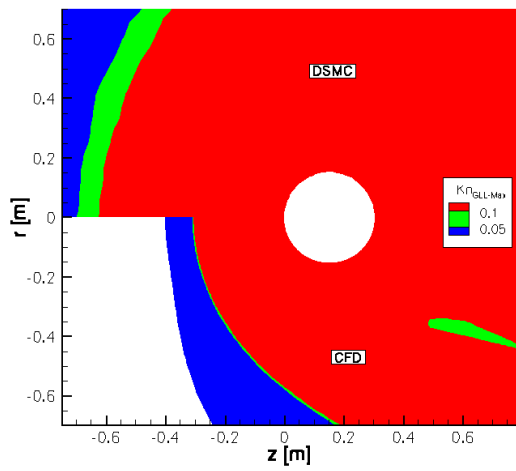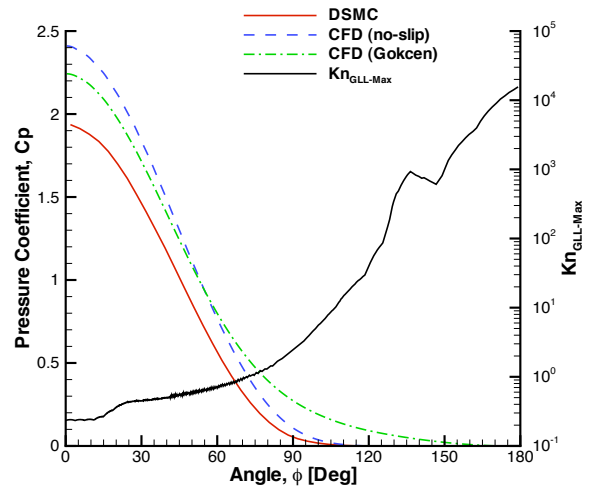
(a) Kn_{GLL}

(b) Coefficient of Pressure

Figure 11. $Kn_\infty = 0.25$, Kn_{GLL} **contours, surface pressure (left axis) and** Kn_{GLL} **surface profile (right axis) on a sphere in a Mach 25 flow of reacting air**

(a) Coefficient of Heat Flux

(b) Coefficient of Shear Stress

Figure 12. $Kn_\infty = 0.25$, **surface heat flux (left axis), surface shear stress (left axis) and** Kn_{GLL} **surface profile (right axis) on a sphere in a Mach 25 flow of reacting air**

American Institute of Aeronautics and Astronautics

and oxygen produced at this flow condition. The temperature and gradient length local Knudsen number profiles along the stagnation streamline are given in Fig. 13 (b). It is interesting to note that at this global Knudsen number, the rotational and vibrational temperatures are small in comparison to the translational temperature. At a global Knudsen of 0.25, the gas is rarefied and there are few collisions. Since there are few collisions, the gas cannot achieve thermal equilibrium, and it limits the amount of chemical reactions that can occur.
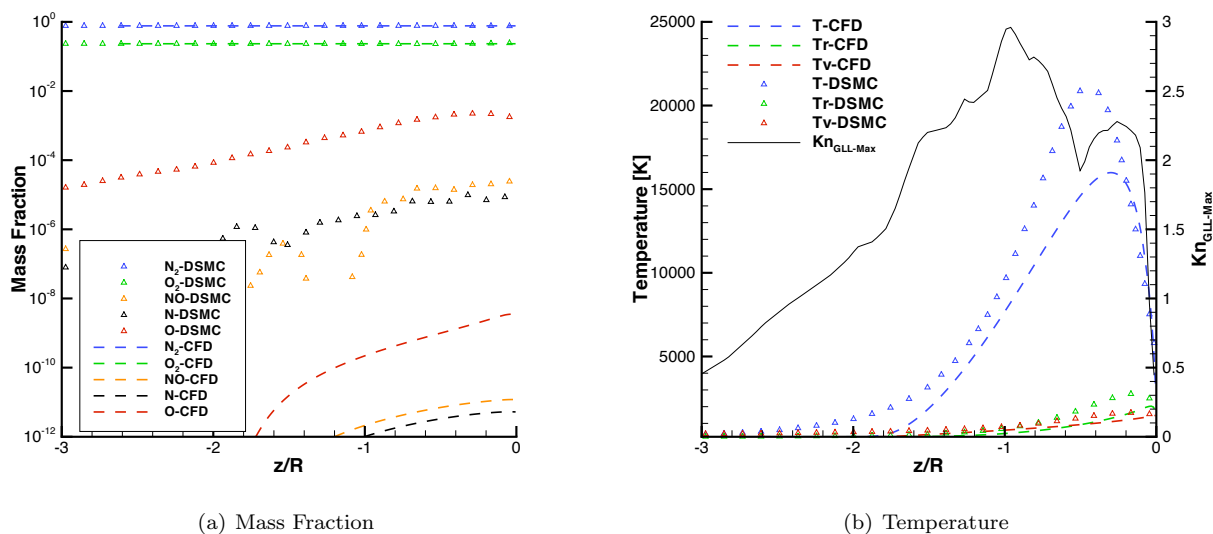

(a) Mass Fraction

(b) Temperature

Figure 13. $Kn_\infty = 0.25$, temperature (left axis), mass fraction (left axis) and Kn_{GLL} (right axis) profiles along the stagnation streamline in a Mach 25 flow of reacting air

V.   Conclusions

This study investigated the effects of continuum breakdown on the surface aerothermodynamic properties (pressure, stress, heat transfer rate) of a sphere in Mach 25 flows in regimes varying from continuum flow to a rarefied gas flow. The first part of this study focused on the effects of reacting flow on continuum breakdown by comparing simulations in nitrogen with and without chemistry. There was little change observed in the surface properties and gradient length local Knudsen number between CFD and DSMC when running these simulations with and without reacting nitrogen flow. The second part of this study looked at the effects of reacting air flow on continuum breakdown and the surface properties of a sphere over a range of global Knudsen numbers varying from continuum to rarefied flow. Differences in peak heat flux and integrated drag between CFD and DSMC were observed to grow with growing global Knudsen number. When slip boundary conditions were employed in the CFD method, the agreement with DSMC improved.

VI.   Future Work

This study focused on the flow of reacting nitrogen and air over a Mach 25 sphere and the effects this had on continuum breakdown and the surface properties of the sphere. The next step is to study the differences in the chemistry models in DSMC and CFD, to be able to better understand the effects on continuum breakdown. The goal is to continue to look at the effects of chemistry, including ionization, on continuum breakdown and the surface properties by studying the same sphere in a Mach 45 flow of reacting air.

Acknowledgments

American Institute of Aeronautics and Astronautics

References

[1] Vincenti, W. G. and Kruger, C. H., *Intorduction to Physical Gas Dynamics*, Krieger Publishing Company, 1965.

[2] Bird, G. A., *Molecular Gas Dynamics and the Direct Simulation of Gas Flows*, Oxford University Press, 1994.

[3] Boyd, I. D., Chen, G., and Candler, G., "Predicting Failure of the Continuum Fluid Equations in Transitional Hypersonic Flows," *Physics of Fluids*, Vol. 7, 1995, pp. 210–219.

[4] Lofthouse, A. J., Scalabrin, L. C., and Boyd, I. D., "Velocity Slip and Temperature Jump in Hypersonic Aerothermodynamics," *Journal of Thermophysics and Heat Transfer*, Vol. 22, No. 1, 2008, pp. 38–48.

[5] Lofthouse, A. J., Boyd, I. D., and Wright, M. J., "Effects of Continuum Breakdown on Hypersonic Aerothermodynamics," *Physics of Fluids*, Vol. 19, 2007, Article 027105.

[6] Lofthouse, A. J., Scalabrin, L. C., and Boyd, I. D., "Hypersonic Aerothermodynamics Analysis Across Nonequilibrium Regimes Using Continuum and Particle Methods," *American Institute of Aeronautics and Astronautics*, 2007, AIAA-2007-3903, 39th AIAA Thermophysics Conference, Miami, Florida, June 25-28.

[7] Holman, T. D. and Boyd, I. D., "Numerical Investigation of the Effects of Continuum Breakdown on Hypersonic Vehicle Surface Properties," *American Institute of Aeronautics and Astronautics*, 2008, AIAA-2008-3928, 40th AIAA Thermophysics Conference, Seattle, Washington, June 23-26.

[8] Dietrich, S. and Boyd, I. D., "Scalar and Parallel Optimized Implementation of the Direct Simulation Monte Carlo Method," *Journal of Computational Physics*, Vol. 126, 1996, pp. 328–342.

[9] Kannenberg, K. C. and Boyd, I. D., "Stategies for Efficient Particle Resolution in the Direct Simulation Monte Carlo Method," *Journal of Computational Physics*, Vol. 157, 2000, pp. 727–745.

[10] Scalabrin, L. C. and Boyd, I. D., "Development of an Unstructured Navier-Stokes Solver for Hypersonic Nonequilibrium Aerothermodynamics," *American Institute of Aeronautics and Astronautics*, 2005, AIAA 2005-52035, 38th AIAA Thermophysics Conference, Toronto, Canada, June.

[11] Scalabrin, L. C. and Boyd, I. D., "Numerical Simulation of Weakly Ionized Hypersonic Flow for Reentry Configurations," *American Institute of Aeronautics and Astronautics*, 2006, AIAA 2006-3773, 9th AIAA/ASME Joint Thermophysics and Heat Transfer Conference, San Francisco, CA, June.

[12] Schwartzentruber, T. E., Scalabrin, L. C., and Boyd, I. D., "Hybrid Particle-Continuum Simulations of Non-Equilibrium Hypersonic Blunt Body Flow Fields," *American Institute of Aeronautics and Astronautics*, 2006, AIAA 2006-3602, 9th AIAA/ASME Joint Thermophysics and Heat Transfer Conference, San Francisco, CA, June.

[13] Boyd, I. D., "Analysis of Vibrational-Translational Energy Transfer using the Direct Simulation Monte Carlo Method," *Physics of Fluids A*, Vol. 3, No. 7, 1991, pp. 1785–1791.

[14] Millikan, R. C. and White, D. R., "Modeling Backward Chemical Rate Processes in the Direct Simulation Monte Carlo Method," *Physics of Fluids*, Vol. 39, 1963, pp. 3209–3213.

[15] Park, C., "Review of Chemical-Kinetic Problems of Future NASA Missions, I: Earth Entries," *Journal of Thermophysics and Heat Transfer*, Vol. 7, No. 3, 1993.

[16] Park, C., *Nonequilibrium Hypersonic Aerothermodynamics*, John Wiley and Sons, 1990.

[17] Lumpkin, F. E., Haas, B. L., and Boyd, I. D., "Resolutions of Differences Between Collision Number Definitions in Particle and Continuum Simulations," *Physics of Fluids A*, Vol. 3, No. 9, 1991.

[18] Farbar, E., "Testing the vibrational relaxation model in MONACO," *Unpublished Report, Department of Aerospace Engineering, University of Michigan*, March 2007.

[19] Deschenes, T. R., Holman, T. D., Boyd, I. D., and Schwartzentruber, T. E., "Analysis of Internal Energy Transfer within a Modular Particle-Continuum Method," *American Institute of Aeronautics and Astronautics*, 2009, AIAA-2009-1213, 47th AIAA ASM Conference, Orlando, Florida, January 5-8.

[20] Gimelshein, N. E., Gimelshein, S. F., and Levin, D. A., "Vibrational Relaxation Rates in the Direct Simulation Monte Carlo Method," *Physics of Fluids*, Vol. 14, No. 12, 2002.

[21] Boyd, I. D., "Modeling Backward Chemical Rate Processes in the Direct Simulation Monte Carlo Method," *Physics of Fluids*, Vol. 19, 2007.

[22] Haas, B. L. and Boyd, I. D., "Models for Direct Monte Carlo Simulation of Coupled Vibration-Dissociation," *Physics of Fluids A*, Vol. 5, No. 2, 1993.

[23] Boyd, I. D. and Gokcen, T., "Computation of Axisymmetric and Ionized Flows using Particle and Continuum Methods," *AIAA Journal*, Vol. 32, 1994, pp. 1828.

Table 6. Reaction Rates Employed in DSMC and CFD

Reaction	a $[m^3/molecule/s]$	η	ε/k_{BOLTZ} [K]
Dissociation			
$N_2 + M \rightleftharpoons N + N + M$ ($M = N_2, O_2, NO$)	1.162×10^{-8}	-1.6	113,200
$N_2 + M \rightleftharpoons N + N + M$ ($M = N, O$)	4.980×10^{-8}	-1.6	113,200
$O_2 + M \rightleftharpoons O + O + M$ ($M = N_2, O_2, NO$)	3.321×10^{-9}	-1.5	59,400
$O_2 + M \rightleftharpoons O + O + M$ ($M = N, O$)	1.660×10^{-8}	-1.5	59,400
$NO + M \rightleftharpoons N + O + M$ ($M = N_2, O_2, NO$)	8.302×10^{-15}	0.0	75,500
$NO + M \rightleftharpoons N + O + M$ ($M = N, O$)	1.826×10^{-13}	0.0	75,500
Exchange			
$NO + O \rightleftharpoons O_2 + N$	1.395×10^{-17}	0.0	19,450
$N_2 + O \rightleftharpoons NO + N$	1.063×10^{-12}	-1.0	38,400